Journal of Cleaner Production xxx (xxxx) xxx

Contents lists available at ScienceDirect

Journal of Cleaner Production

journal homepage: www.elsevier.com/locate/jclepro

A practical approach of urban green infrastructure planning to mitigate urban overheating: A case study of Guangzhou

Yafei Wang [a, b], Zhuobiao Ni [a, b], Mengmeng Hu [a], Shaoqing Chen [a, b, *], Beicheng Xia [a, b, **]

[a] School of Environmental Science and Engineering, Sun Yat-sen University, 135 Xingang Xi Road, 510275, Guangzhou, China
[b] Guangdong Provincial Key Lab of Environmental Pollution Control and Remediation Technology, Sun Yat-sen University, 135 Xingang Xi Road, 510275, Guangzhou, China

ARTICLE INFO

Article history:
Received 30 July 2020
Received in revised form
28 September 2020
Accepted 4 November 2020
Available online xxx

Handling editor: Zhifu Mi

Keywords:
Urban green infrastructure
Local climate zone
Surface urban heat island
ENVI-met
Guangzhou

ABSTRACT

With the rapid economic development and tremendous urban expansion, cities frequently experience overheating problem. Urban green infrastructure (UGI) has proved effective in alleviating urban warming and enhancing thermal comfort. However, few research has been conducted to determine the proper UGI strategy across scales. Here, we propose a sustainable strategy for UGI planning by synthesizing the local climate zone (LCZ) concept and microclimate simulation, with the goal of ameliorating surface urban heat island (SUHI) and improving thermal comfort in cities. The LCZ map of Guangzhou showed that the major 'built-up land types' concentrated in the central area with high land surface temperature (LST) and intensities of SUHI. The circles (1-km diameter) identified as LCZ 2, 3, and 8 were recognized as planning areas by considering the intensities of SUHI and practicability. Afterward, the simulations of the UGI strategy scenarios at three randomly selected sample sites in LCZ 2, 3, and 8 were carried out using the ENVI-met model. The case study results in Guangzhou showed that increasing the green cover to 10% by adding grove and street trees could be the best adaptation strategy to ameliorate overheating, whereas adding extensive green roofs aggravated SUHI to a certain extent and showed minimal impacts on the thermal comfort at a pedestrian level. We show that it is promising to combine the LCZ concept and ENVI-met simulation in optimizing UGI toward urban overheating mitigation.

1. Introduction

In recent decades, the world has undergone an unprecedentedly fast process of urbanization, with the emergence of highly-populated cities such as megacities (having a population that is > 10 million). Urban heat islands (UHIs) are regarded as one of the prominent environmental features of these megacities and profoundly impact the urban thermal environment and the quality of human life (Arnfield, 2003; Souza et al., 2016; Wang et al., 2020). The magnitude of UHIs mainly depends on the modifications of energy, water exchange and airflow due to changes in urban geometry (Sun et al., 2020; Susca et al., 2011), the substitution of surface materials (Akbari et al., 2001; Zolotokrylin et al., 2020), and the fragmentation and loss of natural elements (Takebayashi and Moriyama, 2007). There are two general types of UHI, namely, surface UHIs (SUHIs) and atmospheric UHIs (AUHIs) (Zhou et al., 2014). To address local thermal comfort, this research focuses on SUHIs that can be estimated with thermal infrared remote sensing techniques; AUHIs can only be calculated from weather station networks.

Urban green infrastructure (UGI) has been proven an effective and practical approach to alleviate SUHIs and enhance thermal comfort through shading, evapotranspiration, and wind-shielding (Amani-Beni et al., 2018; Bartesaghi-Koc et al., 2019; Santamouris, 2014; Wang et al., 2019), and can further promote regional economic performance and prosperity (Kim, 2011; Xu et al., 2018; Pan et al., 2019; Pan et al., 2020). Instead of the conventional impervious pavements, UGIs (street trees, city parks, and rooftop gardens, etc.) can be used as cool pavements to deal with UHI mitigation (Qin, 2015; Mohajerani et al., 2017; Wu et al., 2018, 2020; Chen et al., 2019). Although the current evidence of the thermal benefits of UGI has promoted the application of UGI in sustainable urban

* Corresponding author. School of Environmental Science and Engineering, Sun Yat-sen University, 135 Xingang Xi Road, 510275, Guangzhou, China.
** Corresponding author. Guangdong Provincial Key Lab of Environmental Pollution Control and Remediation Technology, Sun Yat-sen University, 135 Xingang Xi Road, 510275, Guangzhou, China.
E-mail addresses: chenshaoqing@mail.sysu.edu.cn (S. Chen), xiabch@mail.sysu.edu.cn (B. Xia).

https://doi.org/10.1016/j.jclepro.2020.124995
0959-6526/

development, the previous findings have limited influence on UGI planning practices due to complex urban geometry as well as cross-disciplinary and cross-scale barriers (Bartesaghi-Koc et al., 2019; Bowler et al., 2010). The current UGI strategy mainly focuses on either one specific public space (Saaroni et al., 2018; Wang et al., 2019) or the urban scale as a whole (Girma et al., 2019; Norton et al., 2015). More research is needed to determine an efficient UGI strategy across scales, which explores not only the optimal arrangement but also the typologies, abundance, and spatial distribution of UGI at the neighborhood and street level (Lu et al., 2017; Zheng et al., 2018).

Simply establishing UGI in vacant lands is inadequate in planning and constructing green infrastructure in cities (Gavrilidis et al., 2019; Sanches and Pellegrino, 2016). The proper design should consider the best location for the UGI and the best type and density of UGI suited for such a location (Gavrilidis et al., 2019; Votsis, 2017). Furthermore, applying a common language to describe urban landscapes worldwide is an important prerequisite for managing UGI for optimal beneficial effects. This is why the term 'land use and land cover' (LULC) was first used to describe urban landscapes (Al-Saady et al., 2015; Anderson et al., 1976; Fu et al., 2013). However, the LULC concept fails to capture urban heterogeneity at fine scales and completely excludes man-made landforms in vertical space (Cadenasso et al., 2007, 2013; Koc et al., 2017). Stewart and Oke (2012) proposed the concept of the 'local climate zone' (LCZ) as a climate-related classification system that identifies ten 'built-up land types' and seven 'land cover types' based on universally recognized building and landforms. This LCZ scheme has been extensively applied in many studies that mainly investigate the following two topics: 1) classifying land surface properties (Cai et al., 2018; Lee and Oh, 2018; Zheng et al., 2018) and 2) determining the thermal performance of LCZs. For instance, several studies have investigated the thermal conditions of LCZs and reported the magnitude of SUHIs among LCZs (Cardoso and Amorim, 2018; Daramola and Balogun, 2019; Droste et al., 2018; Leconte et al., 2015; Shi et al., 2018), while others have focused on the influence of urban characteristic factors on SUHIs among various LCZs (Daramola and Balogun, 2019; Middel et al., 2014; Nassar et al., 2016; Shi et al., 2018). Nevertheless, the LCZ scheme's potential role of bridging the cross-scale integration of UGI studies, has been limitedly addressed in previous investigations. This novel research direction calls for more scientific attention.

In fact, after classifying the urban landscape into different categories, the LCZ scheme can feasibly and conveniently help to further identify the best locations, types, and density of UGI in urban planning and design practices, if a suitable simulation tool is integrated. Such integration, especially with the microclimatic model, could be profound when addressing environmental problems occurring over urban development. To this end, we attempted to develop a practical approach based on the combination of LCZ scheme and a three-dimensional computational fluid dynamics microclimate model (ENVI-met), for seeking the most effective UGI strategies for ameliorating the likely overheating problem in Guangzhou. Using one of the two megacities in southern China as a typical case, this study applied the LCZ scheme to pinpointed the distribution and magnitude of SUHIs in the whole city. Specific UGI scenarios were then simulated by the microclimate model ENVI-met which also evaluates the cooling and warming potential of different UGI strategies across a range of LCZ types with intensive SUHIs. In summary, this study showcases the application of the LCZ concept in urban planning and design and provides key information for UGI planning to improve the thermal environment in populated cities.

2. Study area

Guangzhou, the capital and largest city of Guangdong Province, is the political, economic, and cultural center of South China; it has a total area of 7,434.4 km^2, a population of 14.5 million, and a GDP of US$ 361.6 billion (2018) (Fig. 1). It experiences a subtropical monsoon climate with short and mild winters, as well as long, hot, and humid summers. The mean annual temperature of Guangzhou is approximately 21–29 °C, with monthly maximum values ranging from 18 °C in January to 33 °C in July. During the past two decades, Guangzhou has experienced rapid economic development and tremendous urban expansion accompanied by remarkable changes in the properties of the underlying land surface, which have enhanced the SUHI effect (Chen et al., 2016). The highly urbanized center of Guangzhou is composed of three older districts (Haizhu, Liwan, and Yuexiu) and one new district (Tianhe). Around the city center, Baiyun, Huangpu, and Panyu are the three districts with mild-urbanization level, while Conghua, Huadu, Nansha, and Zengcheng are the four rural districts with relatively low urbanization. Our study area covers all 11 districts of Guangzhou with different urbanization levels (Fig. 1). These districts compromise a variety of urban forms, including commercial, industrial, agricultural, residential, and natural lands. In particular, Zengcheng and Conghua are classified as Guangzhou's eco-tourism and ecological agriculture areas, which contain large coverage of forestland and farmland. Overall, Guangzhou is a modern city undergoing different levels of urbanization, meanwhile experiencing an overheating problem. Being the center in southern China, Guangzhou serves as a typical example of the urban development of many other cities nearby. Therefore, Guangzhou is selected as a representative city for studying UGI planning by synthesizing the local climate zone (LCZ) concept and microclimate simulation.

3. Materials and methods

3.1. Local climate zone (LCZ) classification

The methods adopted to derive an LCZ classification based on data sources include manual sampling, remote sensing, and GIS (Zheng et al., 2018). Manual sampling is very costly and time-consuming and therefore has not been widely applied to LCZ mapping at the urban scale. GIS-based LCZ classification is the most data-intensive method and can be applied places with sufficient and detailed planning data (Shi et al., 2018). However, a comprehensive set of planning data is not available in many cities, especially in developing countries. Remote sensing provides a rapid and low-cost method of LCZ classification using open-source remote sensing images. To support this method, the World Urban Database and Access Portal Tool (WUDAPT) was developed to generate LCZ maps by analyzing satellite images with semiautomated image classification algorithms (Bechtel et al., 2015). The abridged definitions and surface property values for LCZ are listed in the Supporting Information (Tables S1 and S2).

In this study, an LCZ classification map was constructed for Guangzhou using WUDAPT, following five steps (Fig. 2):

1) Based on the region of interest (ROI), Landsat 8 images of Guangzhou from 2017, 2018, and 2019 that met the criteria of having less than 10% cloud cover and being daytime images (i.e., 23 October 2017, 12 February 2018, 29 October 2019) were downloaded from the U.S. Geological Survey (USGS) website.
2) These satellite images were preprocessed and resampled to 100 m from the original 30 m to represent the spectral signal of the local-scale urban structure instead of that of smaller objects.

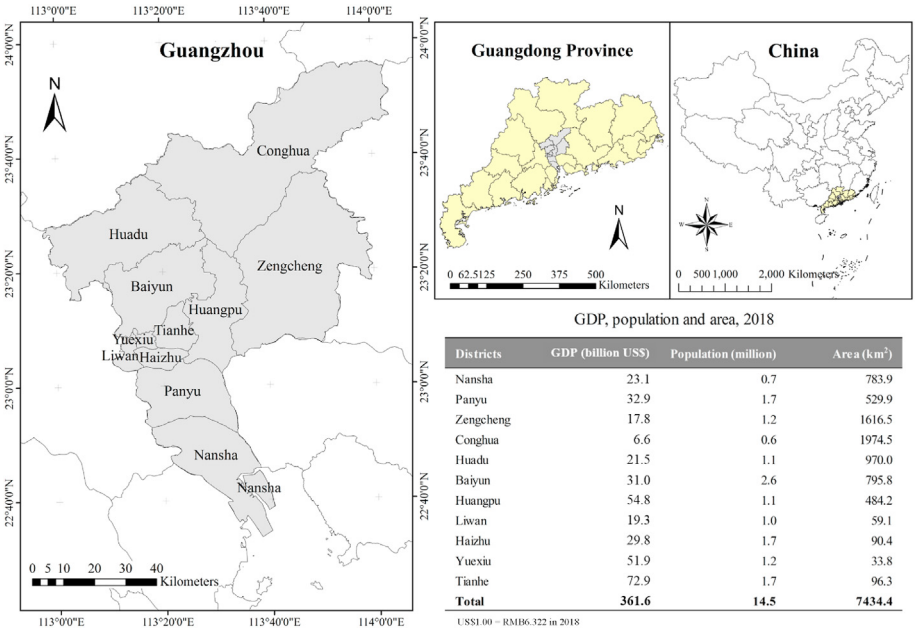

GDP, population and area, 2018

Districts	GDP (billion US$)	Population (million)	Area (km²)
Nansha	23.1	0.7	783.9
Panyu	32.9	1.7	529.9
Zengcheng	17.8	1.2	1616.5
Conghua	6.6	0.6	1974.5
Huadu	21.5	1.1	970.0
Baiyun	31.0	2.6	795.8
Huangpu	54.8	1.1	484.2
Liwan	19.3	1.0	59.1
Haizhu	29.8	1.7	90.4
Yuexiu	51.9	1.2	33.8
Tianhe	72.9	1.7	96.3
Total	**361.6**	**14.5**	**7434.4**

US$1.00 = RMB6.322 in 2018

Fig. 1. Location of Guangzhou, GDP, population, and area in 2018.

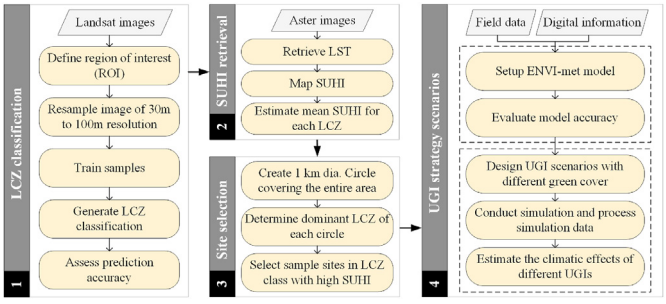

Fig. 2. Technical flow of this study.

3) More than ten training areas for each type of LCZ were digitized and evenly distributed across the study area via Google Earth. The selection principle for the training area followed the guidelines provided by WUDAPT.
4) Based on the Landsat 8 images and the training samples, an LCZ map of Guangzhou was generated using a random forest (RF) classification method in SAGA-GIS.
5) Finally, a set of accuracy assessment points in which each class had the same number of points was generated. To assess the accuracy of the LCZ classification, the predicted and observed LCZ types at the selected points were compared and evaluated with an error matrix or a so-called confusion matrix. Two indices, the overall accuracy (OA) and the Kappa coefficient, were used to assess the accuracy of the LCZ mapping results.

3.2. Surface urban heat island (SUHI) retrieval

SUHIs can be either directly measured or characterized by land surface temperature (LST) (Moyer, 2016) (Text S1). This study retrieved the LST via the single-channel approach using ASTER images of Landsat 8 on 29 October 2019 at the local time of 10:52 a.m. (Jiménez-muñoz et al., 2009; Jiménez-Munoz and Sobrino, 2003). The procedure involved converting pixel values to spectral radiance values, transforming the spectral radiance values to the brightness temperature, and finally estimating the LST values using the brightness temperature (Jiménez-Munoz and Sobrino, 2003; Sobrino et al., 2008). Since a SUHI represents the temperature difference between urban and rural areas, the SUHI value was calculated by subtracting the LST for each pixel from the mean value of a traditional nonurbanized LCZ type (LCZ D: low plants; Table S1) (Shi et al., 2019a,b; Stewart et al., 2014; Yang et al., 2018). Furthermore, the mean SUHI value of each LCZ was calculated using the following formula:

$$\overline{SUHI_X} = \frac{1}{N}\sum_{i=1}^{N}[LST_{Xi} - mean_D(LST_{Di})] \quad (1)$$

where $\overline{SUHI_X}$ represents the mean SUHI value of LCZ X, i is the index of the pixels (i = 1..., N), N is the total number of pixels for LCZ X, and D stands for LCZ D.

3.3. Site selection according to LCZ

To develop an effective UGI strategy, the sites where the SUHI phenomenon is more obvious were selected according to the following steps. First, 1-km diameter circles were created and placed over the study area. Second, the percentages of each LCZ in each circle were calculated, and the dominant LCZ was determined accordingly. Finally, sample sites were randomly selected in the circles that had a dominant LCZ with high SUHI intensity.

3.4. Urban green infrastructure (UGI) strategy scenarios

3.4.1. Model description, setup, and initialization

A three-dimensional computational fluid dynamics (CFD) microclimate model, ENVI-met, was designed to analyze microclimates based on the fundamental laws of fluid dynamics and thermodynamics. The model allows the simulation of surface-plant-air interactions in an urban environment with a resolution as fine as 0.5 m in space and 1–5 s in time (Bruse and Fleer, 1998). The vegetation model in ENVI-met contains complex 3D vegetation

geometries and simulates the interactions between the plant and the surrounding environment based on the physiological processes of evapotranspiration, photosynthesis, and sensible heat flux. Due to its characteristics, ENVI-met has been widely adopted by researchers throughout the world to evaluate the effectiveness of urban greenery for urban heat mitigation (López-Cabeza et al., 2018; Morakinyo et al., 2018; Perini et al., 2017; Wang et al., 2019).

Here, the latest version of the ENVI-met model (v4.4.4 winter) was adopted to simulate and evaluate the impacts of UGI strategies. According to the size and resolution requirements, the studied sites were fitted into 200 × 200 × 30 grids with a resolution of 5 m × 5 m × 3 m, covering an area of 1000 m × 1000 m. The most stable lateral boundary condition (i.e., forced LBC), which copies the values of the one-dimensional model to the boundary, was selected for temperature, humidity, and turbulence to stabilize the 3D model. Five equidistant nesting grids were used to move the borders as far away as possible from the core area, thereby improving numerical stability (Morakinyo et al., 2018; Roth and Lim, 2017; Wang et al., 2019). The "simple forcing" option was adopted to apply the hourly temperature and humidity profiles onto the model. The input data, including geometry, plant and soil databases, and building properties, were obtained from Google Earth satellite images, LocaSpace Viewer digital map application software, and measurements. For the plant data, the values of height, crown diameter, and leaf area density (LAD) were gained through on-site measurement. In this study, LAD was determined through gap fraction analysis with hemispherical canopy photography to infer the canopy structure and light transmittance (Text S2).

To initialize the simulation and to force hourly temperature and humidity profiles, the meteorological record on 29 October 2019 was derived from the Guangzhou meteorological station (113°31′7.92"E, 23°0′08.27"N) to represent the average value for the city. The model was simulated for 24 h with a 1-h interval. Basic information about the vegetation, the model configuration and the initialization parameter values are shown in Tables S3 and S4.

3.4.2. Quantitative evaluation of model performance

The accuracy of the ENVI-met simulation was examined by comparing the hourly simulated and observed air temperature (Ta) and relative humidity (RH) to 1.5 m above ground level. The correlation coefficient, root mean square error (RMSE), mean absolute error (MAE) and Willmott's index of agreement (d) (ranging from 0 to 1) were calculated to evaluate the simulation performance. Lower RMSE and MAE and the higher coefficient and d values indicate better model performance.

3.4.3. Simulation design and data analysis

To investigate the ability of different UGI strategies to ameliorate the overheating problem, five scenarios were applied to all studied sites, including 1) Current: the current condition of the simulation area; 2) Base: the base condition without green infrastructure; 3) 10% GS: the green cover was increased to 10% by adding grove and street trees; 4) 10% GR: the green cover was increased to 10% by adding green roofs; and 5) 20% GS+GR: the green cover was increased to 20% by combining 10% GS and 10% GR scenarios (Fig. S1). *Ficus microcarpa* and *Ficus microcarpa* cv. 'Golden Leaf', as the major tree and shrub species in the study area, were selected for the implementation of UGI strategies. A mid-sized *Ficus microcarpa* (height: 10 m, crown diameter: 9 m, LAD: 2) and *Ficus microcarpa* cv. 'Golden Leaf' (height: 6 m, crown diameter: 4 m, LAD: 2) were used in the scenarios (Table S5).

In reality, the contributions of different UGI to local cooling, their environmental benefits and their sustainability are not equal. Planning authorities have developed weighting systems to normalize the environmental performance of different types of UGI. Of the weighting systems, the Green Area Ratio, which has been widely utilized throughout the world, such as in Berlin (Germany), Malmo (Sweden), and Seattle (USA) (Keeley, 2011), was adopted in this study. Table S6 shows the relative weighting, area and coverage of the different types of green cover under the UGI scenarios.

The SUHI relief provided in Guangzhou by different UGI strategies was estimated under the assumption that the same effect occurred in unsampled regions within the same LCZ. Geostatistical interpolation of the simulated results from the investigated LCZ was then performed to create continuous maps for the entire study area. Kriging is established on the basis of a continuous model of stochastic spatial variation and uses the variogram model (Mulholland et al., 1998; Oliver, 1996; Waller and Gotway, 2004; Webster and Oliver, 2007). Several kriging interpolation approaches are commonly used to grid the air temperatures and UHI intensity (Goovaerts, 1997; Wong et al., 2004; Berezowski et al., 2015; Brinckmann et al., 2016; Jiang et al., 2019; Nikoloudakis et al., 2020). For instance, Berezowski et al. (2015) and Brinckmann et al. (2016) interpolated the minimum and maximum temperatures for Europe using simple kriging that assumes a known mean value. The assumption by ordinary kriging that the mean value being unknown was implemented for both temperature and temperature anomalies in Bergen, Norway (Varentsov et al., 2020). For the nonstationary regionalized variable, universal kriging or kriging with intrinsic random functions should be used. A universal kriging predictor was applied for microclimate prediction in the Maritimes Provinces of Canada (Menafoglio et al., 2013). In this study, the stable semivariogram model of ordinary kriging was adopted to spatially distribute the cooling effects of the UGI strategies at 11:00 a.m., which was the time closest to when the Landsat image was taken.

Based on the energy balance of the human body, the physiological equivalent temperature (PET) at the pedestrian level (1.5 m) was also estimated to evaluate the thermal environment under different UGI strategies. The configuration of the representative personal characteristics was defined based on census data (Guangzhou, 2016) (Table S7). Subsequently, the PET value was translated into the equivalent grade of physical stress on human beings based on the PET classifications for (sub)tropical regions, as shown in Table S8 (Lin and Matzarakis, 2008; Morakinyo et al., 2018).

4. Results and discussion

4.1. LCZ mapping of Guangzhou

Fig. 3a shows the LCZ map of Guangzhou at 100 m grid resolution based on the Landsat 8 images and the training samples. The overall accuracy was determined to be 66.76% with a Kappa coefficient of 0.6469 (Fig. 3b). This value was in general acceptable compared with those of other studies in high-density areas, such as Yangtze River Delta (0.64), Shanghai (0.66), Hangzhou (0.72) (Cai et al., 2018), Wuhan (0.83) (Xu et al., 2017), and Hongkong (0.58) (Wang et al., 2018). The specific proportions of 17 types of LCZs were analyzed for all 11 districts of Guangzhou (Fig. 3c). LCZ A (dense trees) covers nearly half of the city (46%) and occupies more area in the northern districts, including Conghua, Zengcheng, Huangpu, Huadu, and Baiyun districts. As the major 'built-up land types' were concentrated in the central part of the city, LCZ 1–6 accounted for a large land surface in Yuexiu, Liwan, Haizhu, and Tianhe districts, with proportions of 76%, 57%, 56%, and 46%, respectively. In particular, compact building forms (i.e., LCZ 1–3) accounted for 37%, 32%, 27%, and 18% of the total area of these four districts in the central region. LCZ D (low plants) covered the main

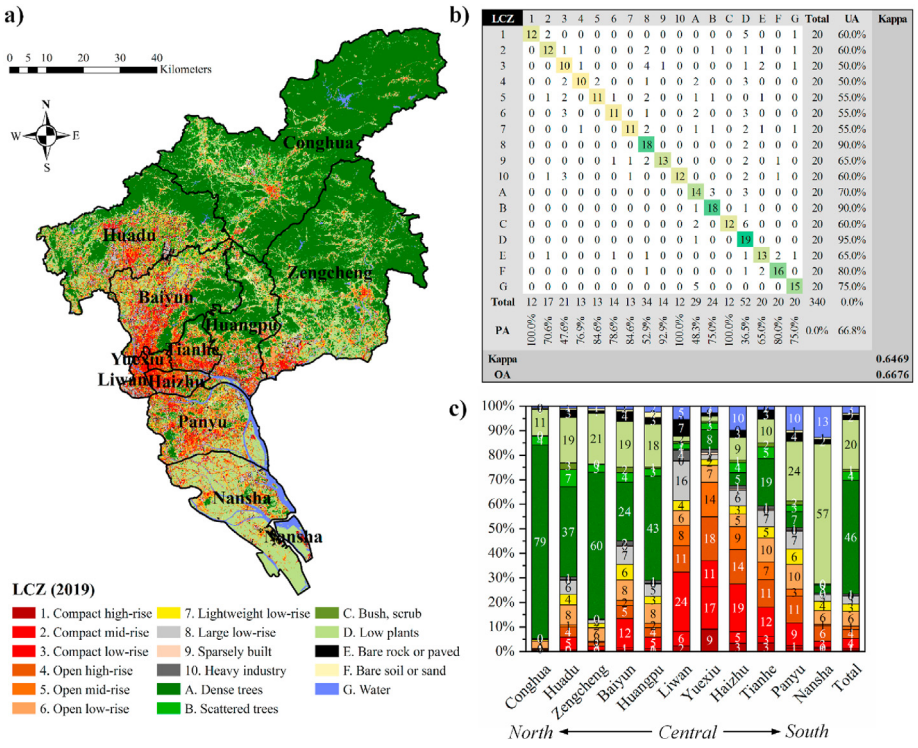

LCZ	1	2	3	4	5	6	7	8	9	10	A	B	C	D	E	F	G	Total	UA	Kappa
1	12	2	0	0	0	0	0	0	0	0	0	0	0	5	0	0	1	20	60.0%	
2	0	12	1	1	0	0	0	2	0	0	0	1	0	1	1	0	1	20	60.0%	
3	0	0	10	1	0	0	0	4	1	0	0	0	0	1	2	0	1	20	50.0%	
4	0	0	2	10	2	0	0	1	0	0	2	0	0	3	0	0	0	20	50.0%	
5	0	1	2	0	11	1	0	2	0	0	1	1	0	0	1	0	0	20	55.0%	
6	0	0	3	0	0	11	0	1	0	0	2	0	0	3	0	0	0	20	55.0%	
7	0	0	0	1	0	0	11	2	0	0	1	1	0	2	1	0	1	20	55.0%	
8	0	0	0	0	0	0	0	18	0	0	0	0	0	0	2	0	0	20	90.0%	
9	0	0	0	0	0	1	1	2	13	0	0	0	0	2	0	1	0	20	65.0%	
10	0	1	3	0	0	0	1	0	0	12	0	0	0	2	0	1	0	20	60.0%	
A	0	0	0	0	0	0	0	0	0	0	14	3	0	3	0	0	0	20	70.0%	
B	0	0	0	0	0	0	0	0	0	0	1	18	0	1	0	0	0	20	90.0%	
C	0	0	0	0	0	0	0	0	0	0	2	0	12	6	0	0	0	20	60.0%	
D	0	0	0	0	0	0	0	0	0	0	1	0	0	19	0	0	0	20	95.0%	
E	0	1	0	0	0	1	0	1	0	0	0	0	0	1	13	2	1	20	65.0%	
F	0	0	0	0	0	0	0	1	0	0	0	0	0	1	2	16	0	20	80.0%	
G	0	0	0	0	0	0	0	0	0	0	5	0	0	0	0	0	15	20	75.0%	
Total	12	17	21	13	13	14	13	34	14	12	29	24	12	52	20	20	20	340	0.0%	
PA	100.0%	70.6%	47.6%	76.9%	84.6%	78.6%	84.6%	52.9%	92.9%	100.0%	48.3%	75.0%	100.0%	36.5%	65.0%	80.0%	75.0%	0.0%	66.8%	
Kappa																				0.6469
OA																				0.6676

Fig. 3. a) LCZ map of Guangzhou at 100 m grid resolution; b) confusion matrix for the LCZ mapping results; c) the proportion of 17 types of LCZ in 11 districts of Guangzhou.

part of southern Guangzhou, mainly in Nansha district. The distribution of the LCZ classes was generally consistent with the actual distribution of land cover observed from the high-resolution Google Earth image.

4.2. Spatial distribution of SUHIs among LCZ classes

The spatial distribution of the LST in Guangzhou on 29 October 2019 at 10:52 a.m. was obtained by applying a single-channel approach, and the SUHI values were retrieved (Fig. 4a). Overall, the LSTs and SUHIs of the 'built-up land types' were generally higher than those of the 'land cover types', with the lowest mean values of 23.2 and −1.1 °C in LCZ G (water), and the highest mean values of 27.4 and 3.0 °C in LCZ 10 (heavy industry), respectively. For the major 'built-up land types' (LCZ 1–6), the LST and SUHI values occurred, in order from high to low, as LCZ 3 > LCZ 2 > LCZ 5 > LCZ 6 > LCZ 4 > LCZ 1 (Fig. 4b). For the rest of the 'built-up land types' (LCZ 7–10), in addition to LCZ 10 (heavy industry), LCZ 8 (large low-rise) also exhibited high LST and SUHI values. In terms of the 'land cover types', LCZ G (water) and A (dense trees) exhibited the lowest LST and SUHI values, whereas LCZ E (bare rock or paved) had the highest values. This finding was generally in line with those in previous studies (Bechtel et al., 2019; Shi et al., 2019a,b), which reported the high intensities of SUHI in LCZs 2, 3, and 8. It is worth noting that LCZ 1 (compact high-rise), with a dense mix of high-rise buildings and few or no trees, had relatively lower intensities of SUHI than LCZ 2 (compact mid-rise) and 3 (compact low-rise). This finding was similar with a study in Guangzhou by Shi et al. (2019a,b), who reported that the orders of the intensities of SUHI from high to low as LCZ 3 > LCZ 2 > LCZ 1. One plausible explanation for this finding is that high-rise buildings create vast shadows that protect the area from direct sunlight. Fig. 4c shows that the whole city generally experienced an overheating problem; 51%–96% of the area had positive SUHI values, especially in the central part of the city. Based on these results, LCZ 2, 3, and 8 were selected for the

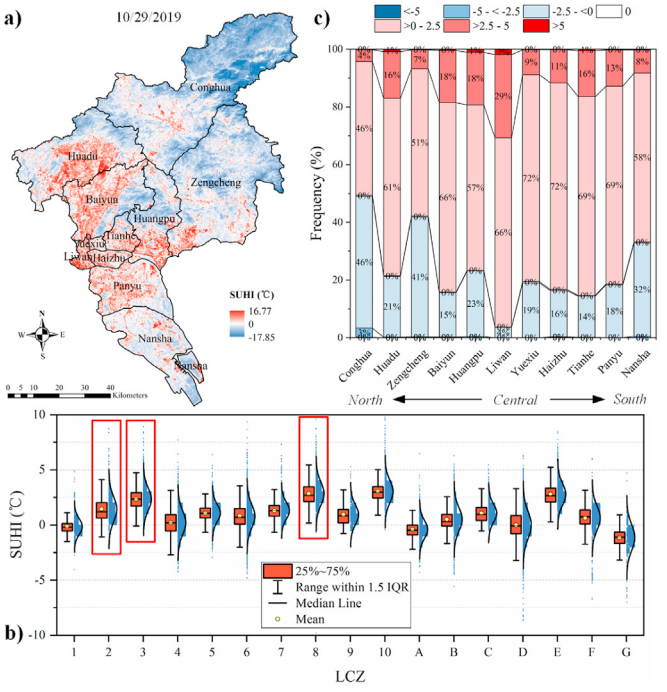

Fig. 4. a) Spatial variation in SUHIs in Guangzhou; b) boxplots of SUHI (°C) for each LCZ class (the upper and lower bounds of the boxplots indicate the 25th and 75th percentile of the values, the interquartile range is 1.5, the black lines show the median value, the yellow points show the mean value, and the blue dots in a half-violin are observation records; the three LCZ planning types are marked by red boxes); c) the frequency of seven classes of SUHI in each district. (For interpretation of the references to colour in this figure legend, the reader is referred to the Web version of this article.)

UGI strategy simulations due to the high intensity of the SUHIs in these LCZ types. Although LCZ 10 and LCZ E (heavy industry and bare rock or paved) also exhibited high SUHI intensity, the UGI strategy is less applicable in these LCZ types, as their functions are not conducive to adding vegetation. Three sample sites were randomly selected from the circles (1-km diameter) that had LCZ 2, 3, and 8 as their dominant LCZ types (Fig. 5).

4.3. Simulation results from UGI strategy scenarios

Fig. 6 displays the land cover characteristics of the sample sites within the simulation domain. According to their Green Area Ratios, the green cover at the LCZ 2, 3, and 8 sites was only 4.48%, 3.53%, and 4.78%, respectively. In contrast, buildings were the dominant components and occupied 32.25%, 48.27%, and 43.03% of the total area of the study sites.

After running a 24-h simulation with a 1-h interval, the simulated Ta and RH at 1.5 m above the ground were extracted for comparison with the measured values at the same location. Overall, a strong agreement was found between the simulation and the measurements for both Ta and RH, with $R^2 > 0.96$, relatively low RMSE and MAE, and $d > 0.90$ for the sample sites (Table S9 and Fig. S2).

4.4. Effects of UGI strategies on LST and SUHI

The effects of different UGI strategies on urban heating mitigation were analyzed by comparing the LST and SUHI values under current, 10% GS, 10% GR, and 20% GS+GR scenarios with those under base scenario. Fig. 7a shows the hourly LST reduction (ΔT_{LST}) over 24 h on 29 October 2019. The different UGI strategy scenarios resulted in variations in LST reduction. During the daytime (6:00 a.m.–6:00 p.m.), the cooling effect of the UGI was obvious at all three sample sites. The average ΔT_{LST} (among LCZ 2, 3, and 8) ranged from −0.16 to −0.18, from −0.31 to −0.39, from −0.15 to −0.17, and from −0.30 to −0.39 °C for current, 10% GS, 10% GR, and 20% GS+GR scenarios, respectively. The maximum ΔT_{LST} reached −0.86, −0.73, and −0.73 °C in LCZ 2, 3, and 8 under 20% GS+GR scenario. On the contrary, adding extensive green roofs (10% GR scenario) aggravated the SUHI to a certain extent, since the ΔT_{LST} under this scenario was lower than that under the current situation for all sample sites. During the early morning hours (1:00 a.m.–5:00 a.m.) and at night (7:00 p.m.–12:00 p.m.), the cooling effect of the green cover was slight and even negative (the value of ΔT_{LST} was positive). One plausible explanation for this result is that the vegetation canopy prevents heat transfer and slows down heat losses at night, thereby increasing the LST and aggravating the SUHI (Akbari, 2002; Wang et al., 2015).

The cooling effect of four different UGI strategy scenarios for the three selected sites was applied in the unsampled region within the same LCZ types (LCZ 2, 3, and 8). The distribution of these planning areas in Guangzhou is shown in Fig. 7b. Fig. 7c displays the average ΔT_{LST} for 11 districts of Guangzhou. The districts located in the central part of Guangzhou (Liwan, Yuexiu, and Haizhu) had a higher average ΔT_{LST} than those in the other parts. This is because the three 'built-up land types' (LCZ 2, 3, and 8) are concentrated in the center of the city. In particular, Liwan exhibited the greatest cooling effects from the UGI strategies, with average ΔT_{LST} values of −0.15 °C (standard deviation SD = 0.03 °C), −0.30 °C (SD = 0.06 °C), −0.14 °C (SD = 0.03 °C), and −0.27 °C (SD = 0.06 °C) for current, 10% GS, 10% GR, and 20% GS+GR scenarios, respectively.

4.5. Effects of UGI strategies on thermal comfort

Fig. 8 illustrates the frequency of different thermal comfort levels under the five scenarios for the three LCZ types separately (Fig. 8a) and together (Fig. 8b). 'Very hot' thermal stress occurred in 7%, 15%, and 11% of the total area in LCZ 2, 3, and 8 under the current conditions and increased to 9%, 18%, and 13% when all the green infrastructure was removed (Base scenario). Moreover, adding grove and street trees (10% GS scenario) reduced the frequency of 'very hot' by approximately 1%, 3%, and 2% compared with that under current situation. Based on de Dear and Fountain (1994) (de Dear and Fountain, 1994), the three moderate categories, i.e.,

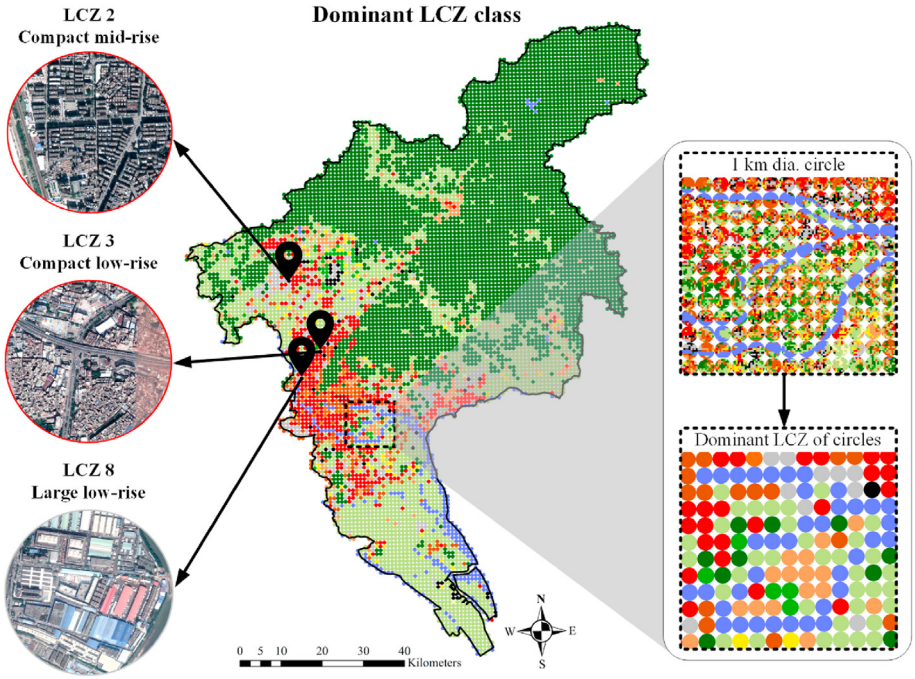

Fig. 5. The dominant LCZ class for each 1-km diameter circle and three sample sites.

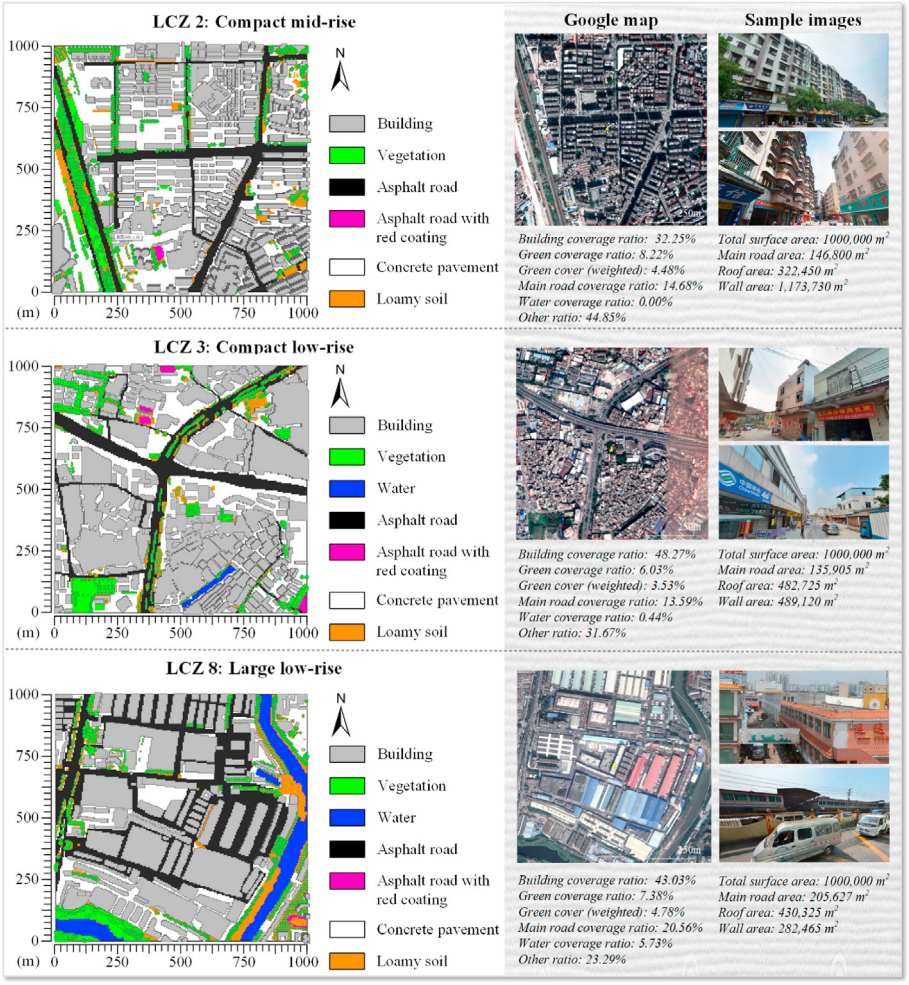

Fig. 6. Images and land cover characteristics of three sample sites within the simulation domain.

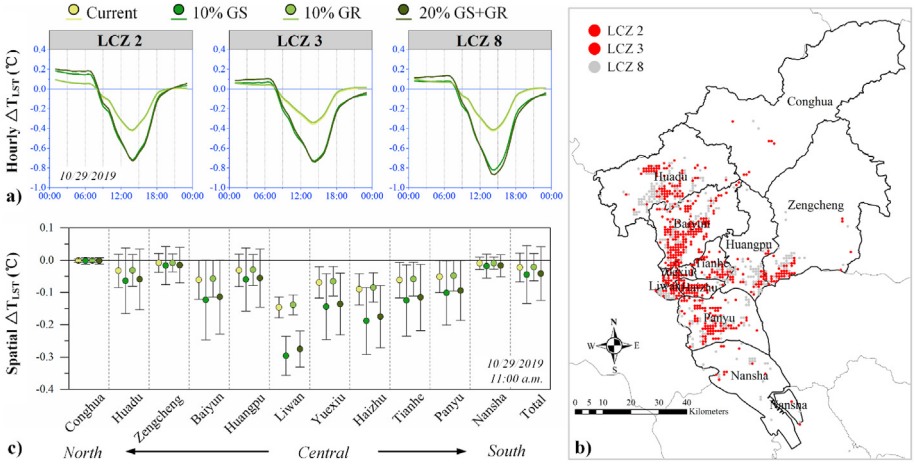

Fig. 7. a) Hourly LST reduction (ΔT_{LST}) over 24 h on 29 October 2019; b) distribution of LCZ 2, 3, and 8 as planning areas in Guangzhou; c) average ΔT_{LST} for 11 districts of Guangzhou (error bars represent the standard deviation).

'slightly cool', 'neutral' and 'slightly warm', were considered to represent 'thermal acceptability'; the percentages of thermal acceptability increased by 1%, 11%, and 7% for LCZ 2, 3, and 8, respectively, under 10% GS scenario. These findings suggest that the UGI plays a more important role in ameliorating heat stress in areas with low-rise buildings than in areas with high-rise buildings. Some other researchers have also reported that green roofs do not present any significant mitigation potential when installed in medium- and high-rise buildings (Chen et al., 2009; Santamouris, 2015; Kim et al., 2018). In addition, the frequency of 'very hot'

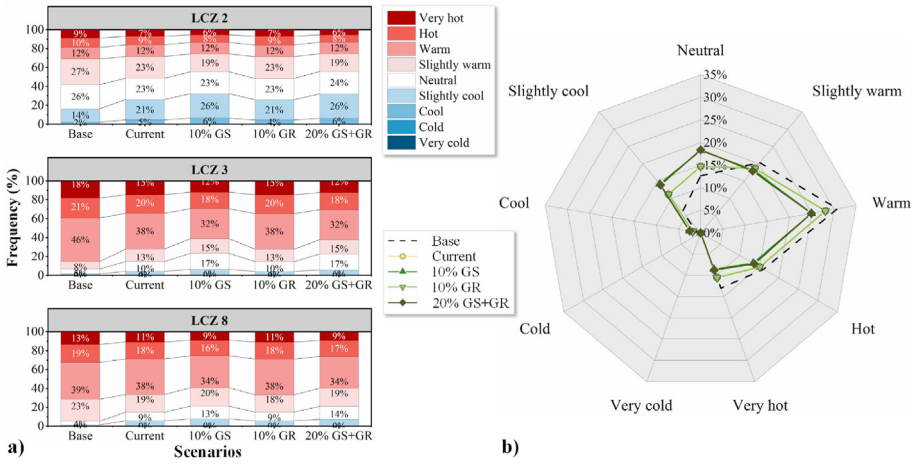

Fig. 8. a) PET frequencies at the pedestrian level under the five UGI scenarios for LCZ 2, 3, and 8 individually; b) Radar map of the overall frequencies of each thermal stress level under the five scenarios.

and thermal unacceptability did not decrease when green roofs were added (10% GR scenario); thus, the impact of the green roofs was limited. Therefore, the effects of combining 10% GS and 10% GR scenarios (20% GS+GR scenario) on heat stress were similar to those of 10% GS scenario and were mainly generated by adding grove and street trees. Such a result is closely related to the poor ΔT_{LST} performance in 10% GR scenario, and agrees with our previous study (Wang et al., 2019), which reported little impact of green roofs on the microclimate and thermal comfort at the pedestrian level. However, urban planners should still consider the contributions of green roofs to building thermal loads and energy consumption, which have been confirmed in a number of investigations (Dordević et al., 2018; Mahmoodzadeh et al., 2020; Peng et al., 2019). The overall performance of different simulated UGI strategies for all three LCZ types also revealed that UGI had a positive impact on thermal comfort by decreasing the frequency of the 'hot' category and increasing the frequency of the 'neutral' category. By this metric, 10% GS scenario performed the best among the three UGI strategies (10% GS, 10% GR, and 20% GS+GR scenarios).

4.6. Limitations and recommendations

The SUHI intensity in the different LCZ types presented in this study generally agrees with those reported in previous studies (Bechtel et al., 2019; Shi et al., 2019a,b). Based on the results and practicability, the three 'representative' sample sites that faced overheating problems were randomly selected from LCZ 2, 3, and 8 for further UGI strategy simulation. However, some LCZ types with high SUHI intensity (i.e., heavy industry, bare rock or paved) were not included due to their functions and uncertainties on land use. The criteria of sample site selection could be improved and become more comprehensive in future studies. For instance, precise characterizations on the actual field conditions of the sites should be performed to determine whether the simulation of some specific LCZ types is required. In addition, the land cover characteristics of the sample sites also restricted the proportions of the added UGI. Considering more detailed and dissimilar UGI addition plans could enhance the accuracy and reliability of the simulation. Moreover, Some popular UGI types, such as vertical green cladding (i.e., green walls), which have spread widely as architectural and constructive elements of building façade design in recent years not included in the study. Due to the substantial differences in façade properties (e.g., height, width, material, isolation, construction) among the different LCZ types, it is difficult to compare them with other selected UGI types in the current research. Not only the types of UGI and LCZ, but also the specific species and field conditions are relevant to the local thermal environment and should be involved in future studies.

4.7. Future perspectives

Guangzhou was selected as the case study city due to its complex urban forms and the property of multi-level of urbanization. In this case, Guangzhou could highly represent other subtropical high-density cities. However, both the types of UGIs and their mitigation effect on urban overheating depend on the climate. The example of Guangzhou might become less representative when dealing with cases with different climate or latitude. This encourages relevant research to be performed in the northern cities or even frigid regions that also suffer from UHI.

The design of UGIs' type and distribution is closely related to land-use and transport developments, and should be coordinated across spatial scales and balance the urban supply and demand (Wu and Plantinga, 2003; Yang et al., 2019; Yang, 2020). Hence, the design of UGIs and their roles in urban heat mitigation should be taken into account in the process of implementing the policy of urban comprehensive planning.

As an important aspect of microclimate regulation, the cooling effect of UGIs has been extensively addressed for seeking proper UGI strategy. Other ecosystem services provided by UGIs, such as air quality regulation, noise abatement, aesthetic information, are as well crucial to achieving sustainable urban development with the help of proper UGI strategy. Besides these benefits, the construction and maintenance of UGIs inevitably incur costs and contribute to environmental impacts throughout the life of UGIs. Hence, future work calls for the analysis of the environmental performances of the different UGI strategies including the costs and benefits throughout their lifespan. While acknowledging the limitations of this study, our findings nevertheless aid policymakers and urban planners in alleviating urban warming and enhancing thermal comfort through the design of UGIs.

5. Conclusions

Finding the most effective UGI strategies across a variety of scenarios is crucial in proposing sustainable urban planning and design for long-term urban heat mitigation. The LCZ scheme has

the potential to bridge the cross-scale integration of UGI studies, yet has been limitedly addressed in previous investigations. Integrating LCZ with a suitable simulation tool can feasibly and conveniently help to further identify the best locations, types, and density of UGI in urban planning and design practices. By synthesizing the LCZ concept and ENVI-met simulation, the present work explored a sustainable UGI strategy to ameliorate SUHI and improve thermal comfort in Guangzhou. The practical approach developed in this work provides a useful guideline for taking into account the role of UGIs with greener urban development.

In general, the major 'built-up land types' (LCZ 1–6) were concentrated in the core urban area, with generally higher LST and SUHI intensity than those of the 'land cover types'. Through comparison, and considering practicability, circular areas (1-km diameter) in LCZs 2, 3, and 8 with high SUHI intensities were selected as planning areas. Based on the simulations of the UGI strategy scenarios at the three randomly selected sample sites in LCZ 2, 3, and 8, it is concluded that increasing the green cover to 10% by adding grove and street trees (10% GS scenario) was the best adaptation strategy for ameliorating the urban overheating. Adding extensive green roofs (10% GR scenario) would aggravate SUHI to a certain extent and have minimal impacts on thermal comfort at a pedestrian level. Overall, this study demonstrates the value of combining the LCZ concept and ENVI-met simulation UGI studies in optimizing UGI toward urban overheating mitigation or other goals.

CRediT authorship contribution statement

Yafei Wang: Conceptualization, Methodology, Software, Formal analysis, Investigation, Writing - original draft, Writing - review & editing, Visualization, Project administration. **Zhuobiao Ni:** Writing - original draft, Writing - review & editing. **Mengmeng Hu:** Software, Investigation. **Shaoqing Chen:** Writing - review & editing, Funding acquisition. **Beicheng Xia:** Supervision, Project administration, Funding acquisition.

Declaration of competing interest

The authors declare that they have no known competing financial interests or personal relationships that could have appeared to influence the work reported in this paper.

Acknowledgments

This research was financially supported by the National Key R&D Program of China (2016YFC0502803), the National Natural Science Foundation of China (41701598, 41703071, 71704015), Natural Science Foundation of Guangdong Province, China (2019A1515011580, 2017A030310532, 2018B030306032), Fundamental Research Funds for the Central Universities (19lgpy163, 19lgzd26).

Appendix A. Supplementary data

Supplementary data to this article can be found online at https://doi.org/10.1016/j.jclepro.2020.124995.

References

Akbari, H., 2002. Shade trees reduce building energy use and CO2 emissions from power plants. Environ. Pollut. 116, S119–S126. https://doi.org/10.1016/S0269-7491(01)00264-0.

Akbari, H., Pomerantz, M., Taha, H., 2001. Cool surfaces and shade trees to reduce energy use and improve air quality in urban areas. Sol. Energy 70, 295–310. https://doi.org/10.1016/S0038-092X(00)00089-X.

Al-Saady, Y., Merkel, B., Al-Tawash, B., Al-Suhail, Q., 2015. Land use and land cover (LULC) mapping and change detection in the little Zab river basin (LZRB), Kurdistan region, NE Iraq and NW Iran. FOG - Freib. Online Geosci. 43, 1–32.

Amani-Beni, M., Zhang, B., Xie, G., Xu, J., 2018. Impact of urban park's tree, grass and waterbody on microclimate in hot summer days: a case study of Olympic Park in Beijing, China. Urban For. Urban Green. 32, 1–6. https://doi.org/10.1016/j.ufug.2018.03.016.

Anderson, J.R., Hardy, E.E., Roach, J.T., Witmer, R.E., 1976. A land use and land cover classification system for use with remote sensor data. In: Geological Survey Professional Paper 964.

Arnfield, A.J., 2003. Two decades of urban climate research: a review of turbulence, exchanges of energy and water, and the urban heat island. Int. J. Climatol. 23, 1–26. https://doi.org/10.1002/joc.859.

Bartesaghi-Koc, C., Osmond, P., Peters, A., 2019. Mapping and classifying green infrastructure typologies for climate-related studies based on remote sensing data. Urban For. Urban Green. 37, 154–167. https://doi.org/10.1016/j.ufug.2018.11.008.

Bechtel, B., Alexander, P.J., Böhner, J., Ching, J., Conrad, O., Feddema, J., Mills, G., See, L., Stewart, I., 2015. Mapping local climate zones for a worldwide database of the form and function of cities. ISPRS Int. J. Geo-Inf. 4, 199–219. https://doi.org/10.3390/ijgi4010199.

Bechtel, B., Demuzere, M., Mills, G., Zhan, W., Sismanidis, P., Small, C., Voogt, J., 2019. SUHI analysis using Local Climate Zones—a comparison of 50 cities. Urban Clim. 28, 100451. https://doi.org/10.1016/j.uclim.2019.01.005.

Berezowski, T., Szcze, M., Kardel, I., Micha, R., Okruszko, T., Mezghani, A., Piniewski, M., 2015. CPLFD-GDPT5 : high-resolution gridded daily precipitation and temperature dataset for two largest Polish river basins. Earth Syst. Sci. Data 8, 1021–1060. https://doi.org/10.5194/essdd-8-1021-2015.

Bowler, D.E., Buyung-Ali, L., Knight, T.M., Pullin, A.S., 2010. Urban greening to cool towns and cities: a systematic review of the empirical evidence. Landsc. Urban Plann. 97, 147–155. https://doi.org/10.1016/j.landurbplan.2010.05.006.

Brinckmann, S., Krähenmann, S., Bissolli, P., 2016. High-resolution daily gridded data sets of air temperature and wind speed for Europe. Earth Syst. Sci. Data 8, 491–516. https://doi.org/10.5676/DWD.

Bruse, M., Fleer, H., 1998. With a three dimensional numerical model. Environ. Model. Software 13, 373–384.

Cadenasso, M.L., Pickett, S.T.A., McGrath, Brian, Marshall, V., 2013. Ecological heterogeneity in urban ecosystems: reconceptualized land cover models as a bridge to urban design. In: Pickett, S.T.A., Cadenasso, M.L., McGrath, B. (Eds.), Resilience in Ecology and Urban Design. Linking Theory and Practice for Sustainable Cities. Springer, New York, pp. 107–129. https://doi.org/10.1007/978-94-007-5341-9.

Cadenasso, M.L., Pickett, S.T.A., Schwarz, K., 2007. Spatial heterogeneity in urban ecosystems: reconceptualizing land cover and a framework for classification. Front. Ecol. Environ. 5, 80–88. https://doi.org/10.1890/1540-9295(2007)5[80:SHIUER]2.0.CO;2.

Cai, M., Ren, C., Xu, Y., Lau, K.K.L., Wang, R., 2018. Investigating the relationship between local climate zone and land surface temperature using an improved WUDAPT methodology – a case study of Yangtze River Delta, China. Urban Clim. 24, 485–502. https://doi.org/10.1016/j.uclim.2017.05.010.

Cardoso, R. dos S., Amorim, M.C. de C.T., 2018. Urban heat Island analysis using the 'local climate zone' scheme in presidente prudente. Braz. Invest. Geogr. 107–118. https://doi.org/10.14198/INGEO2018.69.07.

Chen, H., Ooka, R., Huang, H., Tsuchiya, T., 2009. Study on mitigation measures for outdoor thermal environment on present urban blocks in Tokyo using coupled simulation. Build. Environ. 44, 2290–2299. https://doi.org/10.1016/j.buildenv.2009.03.012.

Chen, J., Chu, R., Wang, H., Zhang, L., Chen, X., Du, Y., 2019. Alleviating urban heat island effect using high-conductivity permeable concrete pavement. J. Clean. Prod. 237, 117722. https://doi.org/10.1016/j.jclepro.2019.117722.

Chen, L., Jiang, R., Xiang, W.N., 2016. Surface heat island in Shanghai and its relationship with urban development from 1989 to 2013. Adv. Meteorol. 2016, 1–15. https://doi.org/10.1155/2016/9782686.

Daramola, M.T., Balogun, I.A., 2019. Local climate zone classification of surface energy flux distribution within an urban area of a hot-humid tropical city. Urban Clim. 29, 100504. https://doi.org/10.1016/j.uclim.2019.100504.

de Dear, R.J., Fountain, M.E., 1994. Field experiments on occupant comfort and office thermal environments in a hot-humid climate. Ashrae Trans. 100, 457–474.

Dordević, K.T., Joksimović, O.D., Jovanović-Popović, M.D., 2018. Energy consumption and CO2 emission reductions trough refurbishment of residential buildings' roofs by applying the Green Roof System - case study. Therm. Sci. 22, S1217–S1230. https://doi.org/10.2298/TSCI170530127D.

Droste, A.M., Steeneveld, G.J., Holtslag, A.A.M., 2018. Introducing the urban wind island effect. Environ. Res. Lett. 13, 1–10. https://doi.org/10.1088/1748-9326/aad8ef.

Fu, Y., Lu, X., Zhao, Y., Zeng, X., Xia, L., 2013. Assessment impacts of weather and land use/land cover (LULC) change on urban vegetation net primary productivity (NPP): a case study in guangzhou, China. Rem. Sens. 5, 4125–4144. https://doi.org/10.3390/rs5084125.

Gavrilidis, A.A., Niță, M.R., Onose, D.A., Badiu, D.L., Năstase, I.I., 2019. Methodological framework for urban sprawl control through sustainable planning of urban green infrastructure. Ecol. Indicat. 96, 67–78. https://doi.org/10.1016/j.ecolind.2017.10.054.

Girma, Y., Terefe, H., Pauleit, S., Kindu, M., 2019. Urban green infrastructure planning in Ethiopia: the case of emerging towns of Oromia special zone surrounding Finfinne. J. Urban Manag. 8, 75–88. https://doi.org/10.1016/j.jum.2018.09.004.

Goovaerts, P., 1997. Geostatistics for natural resources eval- uation. In: Applied Geostatistics Series. Oxford University Press.
Guangzhou, 2016. Guangzhou Statistical Yearbook 2015.
Jiang, P., Liu, X., Zhu, H., Li, Y., 2019. Features of urban heat island in mountainous Chongqing from a dense surface monitoring network. Atmosphere 10, 1–17. https://doi.org/10.3390/atmos10020067.
Jiménez-muñoz, J.C., Cristóbal, J., Sobrino, J.A., Sòria, G., Ninyerola, M., Pons, X., 2009. Revision of the single-channel algorithm for land surface temperature retrieval from Landsat thermal-infrared data. IEEE Trans. Geosci. Rem. Sens. 47, 339–349.
Jiménez-Munoz, J.C., Sobrino, J.A., 2003. A generalized single-channel method for retrieving land surface temperature from remote sensing data. J. Geophys. Res. Atmos. 108, 4688. https://doi.org/10.1029/2003jd003480.
Keeley, M., 2011. The green area ratio: an urban site sustainability metric. J. Environ. Plann. Manag. 54, 937–958. https://doi.org/10.1080/09640568.2010.547681.
Kim, J.H., 2011. Linking land use planning and regulation to economic development: A literature review. J. Plann. Lit. 26, 35–47. https://doi.org/10.1177/0885412210382985.
Kim, H., Gu, D., Kim, H.Y., 2018. Effects of Urban Heat Island mitigation in various climate zones in the United States. Sustain. Cities Soc. 41, 841–852. https://doi.org/10.1016/j.scs.2018.06.021.
Koc, C.B., Osmond, P., Peters, A., 2017. Towards a comprehensive green infrastructure typology: a systematic review of approaches, methods and typologies. Urban Ecosyst. 20, 15–35. https://doi.org/10.1007/s11252-016-0578-5.
Leconte, F., Bouyer, J., Claverie, R., Pétrissans, M., 2015. Using Local Climate Zone scheme for UHI assessment: evaluation of the method using mobile measurements. Build. Environ. 83, 39–49. https://doi.org/10.1016/j.buildenv.2014.05.005.
Lee, D., Oh, K., 2018. Classifying urban climate zones (UCZs) based on statistical analyses. Urban Clim. 24, 503–516. https://doi.org/10.1016/j.uclim.2017.06.005.
Lin, T.P., Matzarakis, A., 2008. Tourism climate and thermal comfort in Sun Moon lake, Taiwan. Int. J. Biometeorol. 52, 281–290. https://doi.org/10.1007/s00484-007-0122-7.
López-Cabeza, V.P., Galán-Marín, C., Rivera-Gómez, C., Roa-Fernández, J., 2018. Courtyard microclimate ENVI-met outputs deviation from the experimental data. Build. Environ. 144, 129–141. https://doi.org/10.1016/j.buildenv.2018.08.013.
Lu, J., Li, Q., Zeng, L., Chen, J., Liu, G., Li, Y., Li, W., Huang, K., 2017. A micro-climatic study on cooling effect of an urban park in a hot and humid climate. Sustain. Cities Soc. 32, 513–522. https://doi.org/10.1016/j.scs.2017.04.017.
Mahmoodzadeh, M., Mukhopadhyaya, P., Valeo, C., 2020. Effects of extensive green roofs on energy performance of school buildings in Four North American climates. Water 12, 1–26. https://doi.org/10.3390/w12010006.
Menafoglio, A., Secchi, P., Dalla Rosa, M., 2013. A Universal Kriging predictor for spatially dependent functional data of a Hilbert Space. Electron. J. Stat. 7, 2209–2240. https://doi.org/10.1214/13-EJS843.
Middel, A., Häb, K., Brazel, A.J., Martin, C.a., Guhathakurta, S., 2014. Impact of urban form and design on mid-afternoon microclimate in Phoenix Local Climate Zones. Landsc. Urban Plann. 122, 16–28. https://doi.org/10.1016/j.landurbplan.2013.11.004.
Mohajerani, A., Bakaric, J., Jeffrey-Bailey, T., 2017. The urban heat island effect, its causes, and mitigation, with reference to the thermal properties of asphalt concrete. J. Environ. Manag. 197, 522–538. https://doi.org/10.1016/j.jenvman.2017.03.095.
Morakinyo, T.E., Lau, K.K.L., Ren, C., Ng, E., 2018. Performance of Hong Kong's common trees species for outdoor temperature regulation, thermal comfort and energy saving. Build. Environ. 137, 157–170. https://doi.org/10.1016/j.buildenv.2018.04.012.
Moyer, A., 2016. Assessing the Urban Heat Island of a Small Urban Area in Central Pennsylvania along the Susquehanna River.
Mulholland, J.A., Butler, A.J., Wilkinson, J.G., Russell, A.G., Tolbert, P.E., 1998. Temporal and spatial distributions of ozone in Atlanta: regulatory and epidemiologic implications. J. Air Waste Manag. Assoc. 48, 418–426. https://doi.org/10.1080/10473289.1998.10463695.
Nassar, A.K., Blackburn, G.A., Whyatt, J.D., 2016. Dynamics and controls of urban heat sink and island phenomena in a desert city: development of a local climate zone scheme using remotely-sensed inputs. Int. J. Appl. Earth Obs. Geoinf. 51, 76–90. https://doi.org/10.1016/j.jag.2016.05.004.
Nikoloudakis, N., Stagakis, S., Mitraka, Z., Kamarianakis, Y., Chrysoulakis, N., 2020. Spatial interpolation of urban air temperatures using satellite-derived predictors. Theor. Appl. Climatol. 141, 657–672.
Norton, B.A., Coutts, A.M., Livesley, S.J., Harris, R.J., Hunter, A.M., Williams, N.S.G., 2015. Planning for cooler cities: a framework to prioritise green infrastructure to mitigate high temperatures in urban landscapes. Landsc. Urban Plann. 134, 127–138. https://doi.org/10.1016/j.landurbplan.2014.10.018.
Oliver, M.A., 1996. Geostatistics, rare disease and the environment. In: Fischer, M.M. (Ed.), Spatial Analytical Perspectives on GIS. Taylor and Francis, London.
Pan, H., Yang, T., Jin, Y., Dall'Erba, S., Hewings, G., 2020. Understanding heterogeneous spatial production externalities as a missing link between land-use planning and urban economic futures. Reg. Stud. https://doi.org/10.1080/00343404.2019.1701186.
Pan, H., Zhang, L., Cong, C., Deal, B., Wang, Y., 2019. A dynamic and spatially explicit modeling approach to identify the ecosystem service implications of complex urban systems interactions. Ecol. Indicat. 102, 426–436. https://doi.org/10.1016/j.ecolind.2019.02.059.
Peng, L.L.H., Yang, X., He, Y., Hu, Z., Xu, T., Jiang, Z., Yao, L., 2019. Thermal and energy performance of two distinct green roofs: temporal pattern and underlying factors in a subtropical climate. Energy Build. 185, 247–258. https://doi.org/10.1016/j.enbuild.2018.12.040.
Perini, K., Chokhachian, A., Dong, S., Auer, T., 2017. Modeling and simulating urban outdoor comfort: coupling ENVI-Met and TRNSYS by grasshopper. Energy Build. 152, 373–384. https://doi.org/10.1016/j.enbuild.2017.07.061.
Qin, Y., 2015. A review on the development of cool pavements to mitigate urban heat island effect. Renew. Sustain. Energy Rev. 52, 445–459. https://doi.org/10.1016/j.rser.2015.07.177.
Roth, M., Lim, V.H., 2017. Evaluation of canopy-layer air and mean radiant temperature simulations by a microclimate model over a tropical residential neighbourhood. Build. Environ. 112, 177–189. https://doi.org/10.1016/j.buildenv.2016.11.026.
Saaroni, H., Amorim, J.H., Hiemstra, J.A., Pearlmutter, D., 2018. Urban Green Infrastructure as a tool for urban heat mitigation: Survey of research methodologies and findings across different climatic regions. Urban Clim. 24, 94–110. https://doi.org/10.1016/j.uclim.2018.02.001.
Sanches, P.M., Pellegrino, P.R.M., 2016. Greening potential of derelict and vacant lands in urban areas. Urban For. Urban Green. 19, 128–139. https://doi.org/10.1016/j.ufug.2016.07.002.
Santamouris, M., 2015. Regulating the damaged thermostat of the cities - status, impacts and mitigation challenges. Energy Build. 91, 43–56. https://doi.org/10.1016/j.enbuild.2015.01.027.
Santamouris, M., 2014. Cooling the cities - a review of reflective and green roof mitigation technologies to fight heat island and improve comfort in urban environments. Sol. Energy 103, 682–703. https://doi.org/10.1016/j.solener.2012.07.003.
Shi, L., Luo, Z., Matthews, W., Wang, Z., Li, Y., Liu, J., 2019a. Impacts of urban microclimate on summertime sensible and latent energy demand for cooling in residential buildings of Hong Kong. Energy 189, 116208. https://doi.org/10.1016/j.energy.2019.116208.
Shi, Y., Lau, K.K.L., Ren, C., Ng, E., 2018. Evaluating the local climate zone classification in high-density heterogeneous urban environment using mobile measurement. Urban Clim. 25, 167–186. https://doi.org/10.1016/j.uclim.2018.07.001.
Shi, Y., Xiang, Y., Zhang, Y., 2019b. Urban design factors influencing surface urban heat island in the high-density city of guangzhou based on the local climate zone. Sensors 19, 1–20. https://doi.org/10.3390/s19163459.
Sobrino, J.A., Jiménez-Muñoz, J.C., Sòria, G., Romaguera, M., Guanter, L., Moreno, J., Plaza, A., Martínez, P., 2008. Land surface emissivity retrieval from different VNIR and TIR sensors. IEEE Trans. Geosci. Rem. Sens. 46, 316–327. https://doi.org/10.1109/TGRS.2007.904834.
Souza, D.O. de, Alvalá, R.C. dos S, Nascimento, M.G. do, 2016. Urbanization effects on the microclimate of Manaus: a modeling study. Atmos. Res. 167, 237–248. https://doi.org/10.1016/j.atmosres.2015.08.016.
Stewart, I.D., Oke, T.R., 2012. Local climate zones for urban temperature studies. Bull. Am. Meteorol. Soc. 93, 1879–1900. https://doi.org/10.1175/BAMS-D-11-00019.1.
Stewart, I.D., Oke, T.R., Krayenhoff, E.S., 2014. Evaluation of the "local climate zone" scheme using temperature observations and model simulations. Int. J. Climatol. 34, 1062–1080. https://doi.org/10.1002/joc.3746.
Sun, F., Liu, M., Wang, Y., Wang, H., Che, Y., 2020. The effects of 3D architectural patterns on the urban surface temperature at a neighborhood scale: relative contributions and marginal effects. J. Clean. Prod. 258, 120706. https://doi.org/10.1016/j.jclepro.2020.120706.
Susca, T., Gaffin, S.R., Dell'Osso, G.R., 2011. Positive effects of vegetation: urban heat island and green roofs. Environ. Pollut. 159, 2119–2126. https://doi.org/10.1016/j.envpol.2011.03.007.
Takebayashi, H., Moriyama, M., 2007. Surface heat budget on green roof and high reflection roof for mitigation of urban heat island. Build. Environ. 42, 2971–2979. https://doi.org/10.1016/j.buildenv.2006.06.017.
Varentsov, M., Esau, I., Wolf, T., 2020. High-resolution temperature mapping by geostatistical kriging with external drift from large-eddy simulations. Am. Meteorol. Soc. 148, 1029–1048. https://doi.org/10.1175/MWR-D-19-0196.1.
Votsis, A., 2017. Planning for green infrastructure: the spatial effects of parks, forests, and fields on Helsinki's apartment prices. Ecol. Econ. 132, 279–289. https://doi.org/10.1016/j.ecolecon.2016.09.029.
Waller, L.A., Gotway, C.A., 2004. Applied spatial statistics for public health data. J. Am. Stat. Assoc. 100, 702–703. https://doi.org/10.1198/jasa.2005.s15.
Wang, R., Ren, C., Xu, Y., Lau, K.K.L., Shi, Y., 2018. Mapping the local climate zones of urban areas by GIS-based and WUDAPT methods: a case study of Hong Kong. Urban Clim. 24, 567–576. https://doi.org/10.1016/j.uclim.2017.10.001.
Wang, Y., Bakker, F., de Groot, R., Wortche, H., Leemans, R., 2015. Effects of Urban Trees on Local Outdoor Microclimate: Synthesizing Field Measurements by Numerical Modelling. Urban Ecosyst. https://doi.org/10.1007/s11252-015-0447-7.
Wang, Y., Ni, Z., Chen, S., Xia, B., 2019. Microclimate regulation and energy saving potential from different urban green infrastructures in a subtropical city. J. Clean. Prod. 226, 913–927. https://doi.org/10.1016/j.jclepro.2019.04.114.
Wang, Yu, Liu, Y., Ye, D., Li, N., Bi, P., Tong, S., Wang, Yan, Cheng, Y., Li, Y., Yao, X., 2020. High temperatures and emergency department visits in 18 sites with different climatic characteristics in China: risk assessment and attributable fraction identification. Environ. Int. 136 https://doi.org/10.1016/j.envint.2020.105486.
Webster, R., Oliver, M.A., 2007. Geostatistics for Environmental Scientists. John

Wiley & Sons, Ltd.
Wong, D.W., Yuan, L., Perlin, S.A., 2004. Comparison of spatial interpolation methods for the estimation of air quality data. J. Expo. Anal. Environ. Epidemiol. 14, 404–415. https://doi.org/10.1038/sj.jea.7500338.
Wu, H., Sun, B., Li, Z., Yu, J., 2018. Characterizing thermal behaviors of various pavement materials and their thermal impacts on ambient environment. J. Clean. Prod. 172, 1358–1367. https://doi.org/10.1016/j.jclepro.2017.10.182.
Wu, H., Yu, J., Song, W., Zou, J., Song, Q., Zhou, L., 2020. A critical state-of-the-art review of durability and functionality of open-graded friction course mixtures. Construct. Build. Mater. 237, 117759. https://doi.org/10.1016/j.conbuildmat.2019.117759.
Wu, J.J., Plantinga, A.J., 2003. The influence of public open space on urban spatial structure. J. Environ. Econ. Manag. 46, 288–309. https://doi.org/10.1016/S0095-0696(03)00023-8.
Xu, C., Haase, D., Pauleit, S., 2018. The impact of different urban dynamics on green space availability: A multiple scenario modeling approach for the region of Munich, Germany. Ecol. Indicat. 93, 1–12. https://doi.org/10.1016/j.ecolind.2018.04.058.
Xu, Y., Ren, C., Cai, M., Edward, N.Y.Y., Wu, T., 2017. Classification of local climate zones using ASTER and Landsat data for high-density cities. IEEE J. Sel. Top. Appl. Earth Obs. Remote Sens. 10, 3397–3405. https://doi.org/10.1109/JSTARS.2017.2683484.
Yang, T., 2020. Understanding commuting patterns and changes: counterfactual analysis in a planning support framework. Environ. Plan. B Urban Anal. City Sci. 1–16. https://doi.org/10.1177/2399808320924433.
Yang, T., Jin, Y., Yan, L., Pei, P., 2019. Aspirations and realities of polycentric development: insights from multi-source data into the emerging urban form of Shanghai. Environ. Plan. B Urban Anal. City Sci. 46, 1264–1280. https://doi.org/10.1177/2399808319864972.
Yang, X., Yao, L., Jin, T., Peng, L.L.H., Jiang, Z., Hu, Z., Ye, Y., 2018. Assessing the thermal behavior of different local climate zones in the Nanjing metropolis, China. Build. Environ 137, 171–184. https://doi.org/10.1016/j.buildenv.2018.04.009.
Zheng, Y., Ren, C., Xu, Y., Wang, R., Ho, J., Lau, K., Ng, E., 2018. GIS-based mapping of Local Climate Zone in the high-density city of Hong Kong. Urban Clim. 24, 419–448. https://doi.org/10.1016/j.uclim.2017.05.008.
Zhou, W., Cadenasso, M.L., Schwarz, K., Pickett, S.T.A., 2014. Quantifying spatial heterogeneity in urban landscapes: integrating visual interpretation and object-based classification. Rem. Sens. 6, 3369–3386. https://doi.org/10.3390/rs6043369.
Zolotokrylin, A.N., Brito-Castillo, L., Titkova, T.B., 2020. Local climatically-driven changes of albedo and surface temperatures in the Sonoran Desert. J. Arid Environ. 178, 104147. https://doi.org/10.1016/j.jaridenv.2020.104147.